

# High-performance hollow sulfur nanostructured battery cathode through a scalable, room temperature, one-step, bottom-up approach

Weiyang Li<sup>a</sup>, Guangyuan Zheng<sup>b</sup>, Yuan Yang<sup>a</sup>, Zhi Wei Seh<sup>a</sup>, Nian Liu<sup>c</sup>, and Yi Cui<sup>a,d,1</sup>

Departments of <sup>a</sup>Materials Science and Engineering, <sup>b</sup>Chemical Engineering, and <sup>c</sup>Chemistry, Stanford University, Stanford, CA 94305; and <sup>d</sup>Stanford Institute for Materials and Energy Sciences, SLAC National Accelerator Laboratory, Menlo Park, CA 94025

Edited by Charles M. Lieber, Harvard University, Cambridge, MA, and approved March 12, 2013 (received for review December 3, 2012)

**Sulfur is an exciting cathode material with high specific capacity of 1,673 mAh/g, more than five times the theoretical limits of its transition metal oxides counterpart. However, successful applications of sulfur cathode have been impeded by rapid capacity fading caused by multiple mechanisms, including large volume expansion during lithiation, dissolution of intermediate polysulfides, and low ionic/electronic conductivity. Tackling the sulfur cathode problems requires a multifaceted approach, which can simultaneously address the challenges mentioned above. Herein, we present a scalable, room temperature, one-step, bottom-up approach to fabricate monodisperse polymer (polyvinylpyrrolidone)-encapsulated hollow sulfur nanospheres for sulfur cathode, allowing unprecedented control over electrode design from nanoscale to macroscale. We demonstrate high specific discharge capacities at different current rates (1,179, 1,018, and 990 mAh/g at C/10, C/5, and C/2, respectively) and excellent capacity retention of 77.6% (at C/5) and 73.4% (at C/2) after 300 and 500 cycles, respectively. Over a long-term cycling of 1,000 cycles at C/2, a capacity decay as low as 0.046% per cycle and an average coulombic efficiency of 98.5% was achieved. In addition, a simple modification on the sulfur nanosphere surface with a layer of conducting polymer, poly(3,4-ethylenedioxythiophene), allows the sulfur cathode to achieve excellent high-rate capability, showing a high reversible capacity of 849 and 610 mAh/g at 2C and 4C, respectively.**

lithium sulfur battery | energy storage | long cycle life

Conventional lithium ion batteries based on carbon anodes and lithium metal oxide cathodes, with theoretical specific energy of about 400 Wh/kg, have now seen the limit of meeting the needs of high-energy storage for applications in portable electronics, vehicle electrification, and grid-scale stationary energy storage (1–4). To achieve a quantum leap in the batteries specific energy density, new electrode materials with high charge storage capacity are needed. Over the past few years, extensive research has been conducted on developing high-capacity electrode materials, including the silicon (Si) anode that has high theoretical capacity of 4,200 mAh/g, 10 times more than that of carbon (370 mAh/g). Various Si nanostructures have been designed to successfully overcome the materials and interface problems, and Si anode with stable cycling up to 6,000 cycles has been reported (5–10). However, the development of high-capacity cathode materials with stable cycling comparable to the anodes has been rather challenging. Sulfur (S) is an exciting cathode material due to its high theoretical capacity of 1,673 mAh/g, large abundance, and low toxicity (11). Combined with the Si or lithium metal anodes, the S-based full batteries can achieve four or five times of the theoretical specific energy of the existing C–LiCoO<sub>2</sub> system (12).

Despite the promise of S cathode, there exist multiple fundamental materials challenges that prevent it from reaching the cycling performance suitable for portable electronics and electrical vehicles (11, 13–16). The rapid capacity decay of S cathode can be attributed to several reasons, including the large volume expansion of S (~80% change) upon lithiation, dissolution of intermediate lithium polysulfides (Li<sub>2</sub>S<sub>x</sub>, 4 ≤ x ≤ 8) in the electrolyte, and low

ionic/electronic conductivity of both S and Li<sub>2</sub>S. To solve these problems, much effort has been devoted to designing novel microstructured/nanostructured materials of S cathodes (17–29). Various carbon nanostructures have been studied as conductive matrix to encapsulate S and trap polysulfides within the carbon frameworks. For example, Nazar and coworkers (17) pioneered the concept of using ordered mesoporous carbon to constrain S within its channels, followed by modification of polyethylene glycol. This approach addressed the conductivity issue and improved polysulfides trapping, resulting in a high reversible capacity of over 1,000 mAh/g at C/10 rate for 20 cycles. Other carbon-based materials that have been used to improve S cathode performance include mesoporous hollow carbon spheres (18, 19), hollow/porous carbon nanofibers (20–22), activated carbon fiber (23), and graphene oxides (24, 25). Recent advancement in further stabilizing S cathode performance was demonstrated by Nazar and coworkers (26, 27), in which mesoporous silica (SBA-15) and titania were used to facilitate the trapping and adsorption of soluble polysulfides. Tarascon and coworkers (28) also generalized the use of polysulfide reservoirs to other mesoporous oxide structure, such as metal–organic framework, demonstrating nearly ~80% capacity retention after 80 cycles. Despite the tremendous progress, there has been little success reported on Li–S batteries with good capacity performance up to 1,000 cycles, which is the Department of Energy requirement for electric-vehicle-grade batteries systems (30). In addition, the fabrication of the carbon-based S composites and mesoporous oxides additives usually require elaborate procedures, involving high-temperature process and corrosive acid for template synthesis. These requirements can significantly limit the manufacturability of the S cathode materials.

Although encapsulation of nanostructured S and attenuation of polysulfide dissolution have been recognized as key points in improving the S cathode performance, the approaches used in the previous reports involve using melting and infusion of S into other materials matrix and have limitation in realizing an S cathode design that can address all of the problems simultaneously. Improving the S cathode performance requires a multifaceted approach that can address the problems at different length scales. Trapping of polysulfides requires appropriate molecular functionalities built into a suitable nanostructure. Engineering empty space into the electrode at the nanoscale can address the problem of volumetric expansion. At the macroscopic scale, electrode homogeneity and integrity have been important in ensuring cathode

Author contributions: W.L. and Y.C. designed research; W.L. carried out materials fabrication; W.L., G.Z., and Y.Y. performed electrochemical tests; W.L. and N.L. performed TGA analysis; and W.L. and Y.C. wrote the paper.

The authors declare no conflict of interest.

This article is a PNAS Direct Submission.

Freely available online through the PNAS open access option.

<sup>1</sup>To whom correspondence should be addressed. E-mail: yicui@stanford.edu.

This article contains supporting information online at [www.pnas.org/lookup/suppl/doi:10.1073/pnas.1220992110/-DCSupplemental](http://www.pnas.org/lookup/suppl/doi:10.1073/pnas.1220992110/-DCSupplemental).

performance (31). These stringent requirements pose significant challenges to the previous top-down approaches of melting and infusing S into the matrix. In many cases, S precipitation on the outer surface of the host matrix could not be avoided. It has been reported by various groups that additional processes (carbon disulfide washing or heating) are needed to remove the inhomogeneously deposited S to avoid rapid capacity decay (15, 20, 32). This problem has also led to great variation in battery performance even with similar electrode structure and composition (25, 26, 28). Most recently, our group demonstrated that a design of S@TiO<sub>2</sub> yolk-shell nanoarchitecture could improve the cycling stability of S cathode due to the void space engineered into the TiO<sub>2</sub> shell to accommodate the S volumetric expansion (33). However, such yolk-shell design still requires elaborate synthetic procedures involving controlled TiO<sub>2</sub> coating and precise chemical etching to dissolve a specific amount of S to generate the internal empty space. It is therefore highly desired to develop a simple and scalable approach to fabricate S cathode that allows precise tuning of the materials, to achieve high capacity over long-term cycling.

Herein, we report a monodisperse, polymer-encapsulated hollow S nanosphere cathode for excellent prolonged cycling stability over 1,000 charge/discharge cycles. The S cathode is fabricated using a scalable, one-step, room temperature, bottom-up approach, which allows unprecedented control over the electrode architecture for addressing the materials issues of S cathode from the nanoscale to macroscale. As shown in Fig. 1A, (i) the S particles are coated with a layer of polymer shell of polyvinylpyrrolidone (PVP) that can minimize the polysulfides dissolution; (ii) empty space has also been engineered into the particles for S to expand inward instead of outward upon lithiation; (iii) the S nanoparticles have small dimensions to facilitate electron and ion transport; (iv) the monodispersity of the S nanospheres can promote a more homogeneous mixing of S in the electrode, minimizing the formation of large, electrically isolated S chunks, and thus allowing for intimate contact with conductive additive (carbon black). Using PVP-encapsulated hollow S nanospheres, we demonstrate high specific discharge capacities at different current rates (1,179,

1,018, and 990 mAh/g at C/10, C/5, and C/2, respectively) and excellent capacity retention of 77.6% (at C/5) and 73.4% (at C/2) after 300 and 500 cycles, respectively. A capacity decay as low as 0.046% per cycle and an average coulombic efficiency of 98.5% was presented over a long-term cycling of 1,000 cycles at C/2. In addition, by simply modifying the S nanosphere surface with a layer of conducting polymer, poly(3,4-ethylenedioxythiophene), the S cathode exhibited excellent rate capability. Even discharged/charged at high rates of 2C and 4C, a high reversible capacity of 849 and 610 mAh/g can be achieved, respectively.

## Results and Discussion

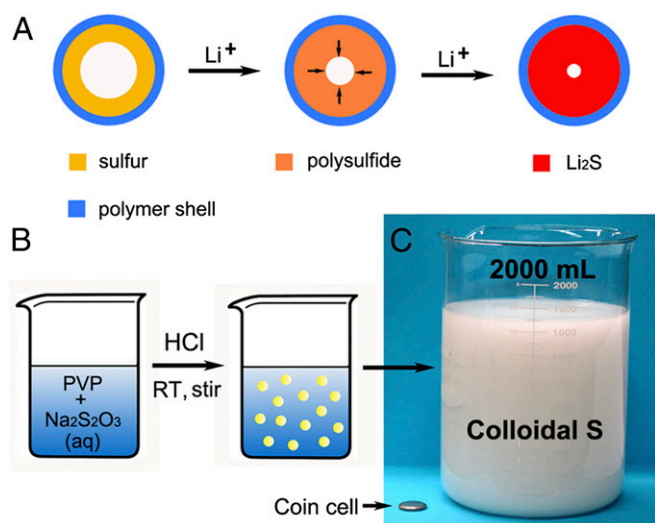
The synthesis of monodisperse polymer-encapsulated S nanospheres is based on a simple reaction between sodium thiosulfate and hydrochloric acid in an aqueous solution in the presence of PVP at room temperature. The reaction can be written as the following:



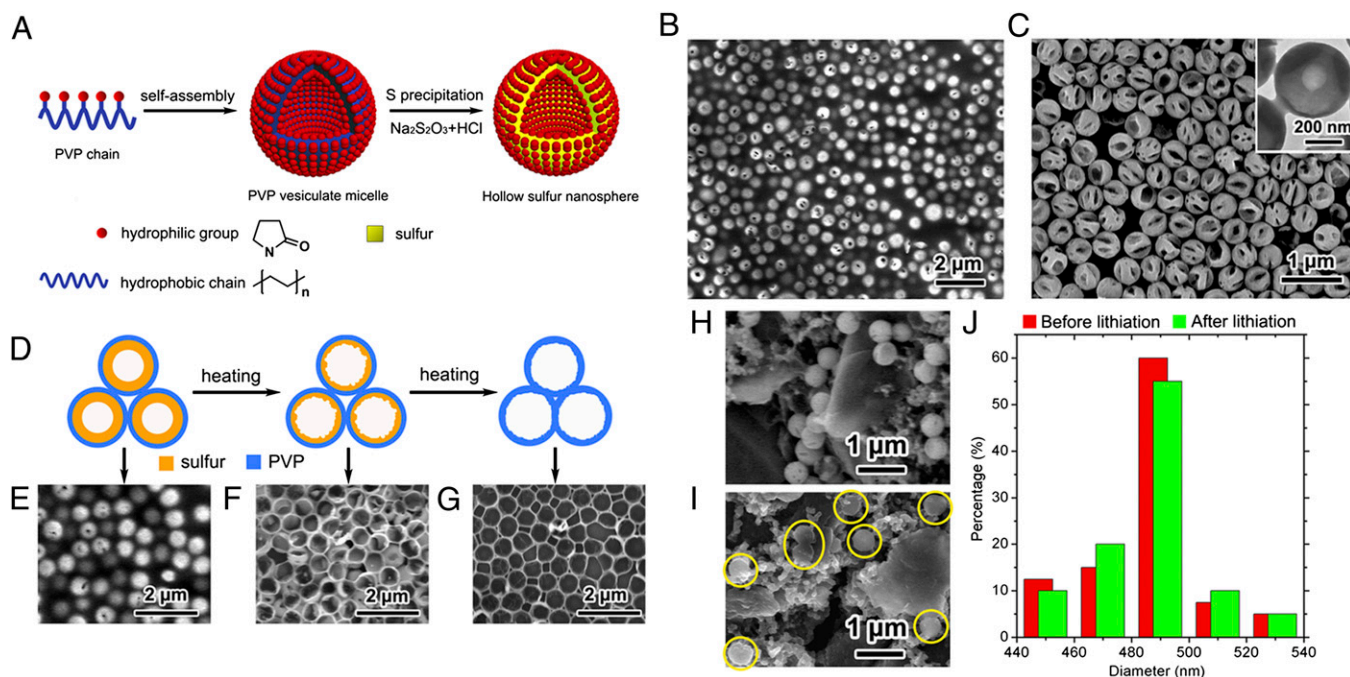
Compared with the existing approaches for S cathode fabrication, our bottom-up synthesis of S nanospheres offers several advantages. (i) The S nanospheres are highly uniform with a layer of PVP polymer coating that can help trap polysulfide dissolution. (ii) The synthesis was carried out at room temperature with a single step (Fig. 1B). Such a process can be straightforward to scale up in industry. The process is environmentally benign and highly reproducible. In our laboratory, this method can easily produce hollow S nanospheres with high quality in large quantities (on a scale of gram per batch in a beaker) (Fig. 1C). (iii) The use of these particles in battery electrodes is compatible with traditional lithium ion battery manufacturing technique by using conventional conductive additive, binder, and electrolyte.

Fig. 2A schematically illustrates the formation mechanism for the PVP-encapsulated hollow S nanospheres. PVP not only functions as a capping agent to control the particle growth and ensure monodispersity of particle size but also acts as a soft template for the formation of unique hollow structures. Dynamic light scattering has shown that PVP nanoaggregates were found to exist in PVP aqueous solution (34). A recent study by Mao and coworker (35) showed that the PVP molecules can interact with each other in aqueous solution to form hollow microspheres due to a self-assembly process. PVP had also been used as soft template for synthesizing hollow spheres of conductive polymers (36). In aqueous solution, both the polymer backbone (blue) and the methylene groups in the five-member ring of PVP can enable the association of PVP molecules through hydrophobic interaction, while the electronegative amide groups (red dots) are effectively linked together through the hydrogen bond network of water (34–36). Therefore, it is expected that the PVP molecules could self-assemble into a hollow spherical vesicular micelle with a double-layer structure, having their hydrophobic alkyl backbones pointed toward the interior of the micelle wall and the hydrophilic amide group outward into the water (Fig. 2A). When S started to form in the beginning of the reaction, its hydrophobic nature made it grow preferentially onto the hydrophobic portion of the PVP micelles. These micelles serve as soft template to direct the growth of hollow S nanospheres. Because of the interaction between S and PVP and the highly hydrophobic nature of S, many PVP molecules could further absorb on the S nanoparticle surface if S is exposed to water during growth, forming a dense layer of polymer coating during the particle synthesis. That is, S is located in the interior of the hollow particle wall and is isolated from the water by PVP.

Fig. 2B and C show typical scanning electron microscopy (SEM) images of the PVP-encapsulated hollow S nanospheres. These SEM images show several key features of these nanospheres. First, the particle size is highly monodispersed. A statistic counting



**Fig. 1.** Schematic illustrations of the structure and fabrication process of PVP-encapsulated hollow S nanospheres. (A) Schematic showing the structure of PVP-encapsulated S nanosphere with empty space inside and the inward expansion during lithiation for the accommodation of volume change and the confinement of polysulfides by the shell. (B) The fabrication process of PVP-encapsulated hollow S nanospheres based on a simple reaction between sodium thiosulfate and hydrochloric acid in an aqueous solution in the presence of PVP at room temperature (RT). (C) Digital camera image of the synthesis scaled up in a 2,000-mL beaker (on a scale of gram per batch).



**Fig. 2.** Fabrication, characterization, and lithiation of PVP-encapsulated hollow S nanospheres. (A) Schematic of the formation mechanism for PVP-encapsulated hollow S nanospheres. (B) SEM image of the as-prepared PVP-encapsulated hollow S nanospheres. (C) SEM image of the hollow S nanospheres after washing them with water to remove the PVP on the particle surface. (C, *Inset*) TEM image of an individual hollow S nanospheres. (D) Schematic diagram illustrating the subliming process of the PVP-encapsulated hollow S nanospheres. (E–G) SEM images of the S particles (E) before, (F) during, and (G) after S sublimation, respectively. (H and I) Typical SEM images of S nanospheres on the conducting carbon-fiber paper (H) before and (I) after lithiation. The particles after lithiation were marked with yellow circles in I. (J) A comparison of the size distribution of S nanospheres before and after lithiation.

over 200 S particles in a synthesis batch (Fig. S1) shows that the diameters of  $\sim 95\%$  of particles are in the range of 400–460 nm. Between different batches of synthesis, the monodispersity of particle size is reproducible with the average diameter only shifted slightly within the window of 400–500 nm. Second, the particles have hollow interior structure. This characteristic was also confirmed by the distinct contrast shown in the transmission electron microscopy (TEM) image (Fig. 2C, *Inset*). It is noted that many of the S particles have small pores in their walls besides the large empty space in the middle. This could be due to the  $\text{SO}_2$  bubbles generated during the particle synthesis accompanying with S precipitation (Eq. 1). However, despite the pores inside the S wall, all S is still isolated from the outside aqueous solution by PVP due to the hydrophobic nature of S.

To further understand the formation mechanism of hollow S nanospheres, various polymers and surfactants, including polyvinyl alcohol (PVA), polydiallyldimethylammonium chloride (polyDADMAC), polyethylene glycol (PEG), and sodium dodecylbenzenesulfonate (SDBS) were investigated (Fig. S2). Both PVA and polyDADMAC could also assist the growth of uniform S nanospheres with different sizes and surface characteristics, whereas PEG and SDBS could not controllably manipulate the shape of the resulting S particles. From the structures of these polymers (Fig. S2, *Insets*), we can see that both PVA and polyDADMAC have a similar structural configuration as PVP, consisting of a hydrophobic carbon backbone and a branched hydrophilic moiety in each repeating unit, whereas PEG has hydrophilic hydroxyl groups at both ends of the polymer chain. Therefore, the formation of nanospheres from PVA and polyDADMAC can be explained in a similar fashion, with the help of the formation of micelles, directing the growth of S. The reason why PEG did not work was due to its incapability to form micelles. As to SDBS, a small molecule, the interaction between the much

shorter carbon chains compared with that of the polymers is not strong enough to provide sufficient stability for S growth.

To confirm the PVP shells on the S particles, we drop-casted S nanoparticle suspension on a Si substrate, followed by heating in vacuum and analyzing under SEM. Fig. 2D shows a schematic illustrating the S subliming process of the PVP-encapsulated hollow S nanospheres. Fig. 2E–G displays the corresponding SEM images of the sample before, during, and after S sublimation, respectively. After all of the S had been sublimed (confirmed by energy-dispersive X-ray analysis showing no S signal), the PVP shells ( $\sim 29$  nm in thickness) surrounding the particles can be clearly resolved (Fig. 2G). Thermal gravimetric analysis (Fig. S3) reveals that the amount of elemental S in the sample is 70.4 wt%. From the weight percentage of S, particle size, and thickness of PVP shell, we can estimate that the pore volume inside each particle is  $\sim 54.3\%$  of the S wall volume (see calculation in *SI Text*). Assuming the volume expansion is linearly dependent on the degree of lithiation, this pore volume would allow 68% of theoretical capacity or 1,138 mAh/g to be used if only inward volume expansion is considered. The variations in the X-ray photoelectron spectroscopy of the PVP-encapsulated hollow S nanospheres and the pure elemental S were shown in Fig. S3. For pure S, two peaks positioned at 163.9 and 165.1 eV can be assigned to the S  $2p_{3/2}$  and S  $2p_{1/2}$ , respectively. As to hollow S nanospheres, the S peak shifts to a higher binding energy with its core level located at 167 eV and exhibits a much broader full widths at half-maximum, indicating partial charge transfer of S to PVP (37). This result clearly shows the interaction between PVP and S, which could contribute to the effective trapping of polysulfides and thus result in the outstanding capacity retention.

To evaluate whether there is any volume expansion outward of the PVP-encapsulated hollow S nanospheres after lithiation, the S nanosphere suspension was drop-casted on a piece of conducting carbon-fiber paper (used as substrate) without the addition

of carbon black and binder, and then dried in vacuum overnight. A pouch cell was assembled in an Ar-filled glove box using the carbon fiber paper with S particles as cathode and Li foil as anode. The cell was discharged at a current rate of C/5 to 1.5 V, and then the voltage was held at 1.5 V for  $\sim 18$  h. A typical two-plateau voltage profile of the S cathode can be observed (Fig. S4), indicating that lithium ions can penetrate through the PVP shell and react with the inner S during lithiation. After the first lithiation, the carbon-fiber paper cathode from the cell was retrieved and washed with 1,3-dioxolane. Typical SEM images of the PVP-encapsulated hollow S nanospheres on the carbon-fiber paper substrate before and after lithiation are shown in Fig. 2*H* and *I*. Fig. 2*J* presents the size distribution of the S particles before and after lithiation. We can see that the particles after lithiation still preserved nearly a spherical shape (Fig. 2*I*, marked by yellow circles) and no obvious size difference was observed between the particles before and after lithiation [average diameter, 483 nm (before) and 486 nm (after)]. This indicates that S expands inward into the hollow space, and the polymer shell is mechanically rigid enough to avoid outward expansion or breakage, and thus can effectively limit the polysulfides from diffusing into the electrolyte.

To test the electrochemical performance, 2032-type coin cells were assembled using a metallic Li foil as anode.  $\text{LiNO}_3$  was added to the electrolyte as additive because it has been shown to passivate the lithium anode surface and thus reduce the shuttle effect (15, 37). The specific capacities were calculated based on the S mass only. The typical mass loading of active S was  $\sim 1$  mg/cm<sup>2</sup>.

Fig. 3*A* shows the typical discharge–charge voltage profiles of the cells made from the PVP-encapsulated, hollow S nanospheres at different current rates (C/10, C/5, and C/2, where 1C = 1,673 mA/g) in the potential range of 2.6–1.5 V at room temperature, showing the highest discharge capacities achieved at different current rates. At C/10, a capacity of 1,179 mAh/g can be obtained, whereas at higher discharge rates of C/5 and C/2, the electrode delivered a capacity of 1,018 and 990 mAh/g, respectively. The discharge profiles of all three current densities were characterized by a two-plateau behavior of a typical S cathode. Fig. 3*B* shows the cycling performances of the cells made from the PVP-encapsulated hollow S nanospheres at C/5 rate for 300 cycles. Contrary to the previous studies where rapid initial decay was observed, the discharge capacity exhibited a gradual increase during the first several cycles, indicating an activation process for the electrodes. This could be explained by the increase in the accessibility of S materials to the electrolyte during the cycling process. Because of the PVP shell, it took some time for S to get into contact with the electrolyte and become fully electrochemically active. Similar activation process was also observed for polyaniline-encapsulated S nanotubes (29). Electrochemical impedance spectroscopy (EIS) measurements were carried out at different discharge states of the 1st, 5th, and 10th cycle during the activation (Fig. S5). Two depressed semicircles were observed during the discharge process. The semicircle in the high-frequency (HF) region could reflect the charge transfer process at the conductive agent interface, whereas the semicircle in the middle-frequency (MF) range could be attributed to the formation of insoluble polysulfide species (38). Previous studies showed that the impedance of interfacial charge transfer dominates the reduction reaction during upper voltage plateau, whereas the mass transport dominates the lower voltage plateau (15, 38). During the activation of the electrode from the 1st to the 10th cycle, at the upper discharge voltage plateau, the HF semicircle resistance decreases, showing faster interfacial charge transfer; whereas at the lower voltage plateau, the MF semicircle resistance increases, indicating more formation of insoluble  $\text{Li}_2\text{S}_2/\text{Li}_2\text{S}$ . At C/5 rate, an initial capacity of about 792 mAh/g was achieved. After several cycles of activation, the

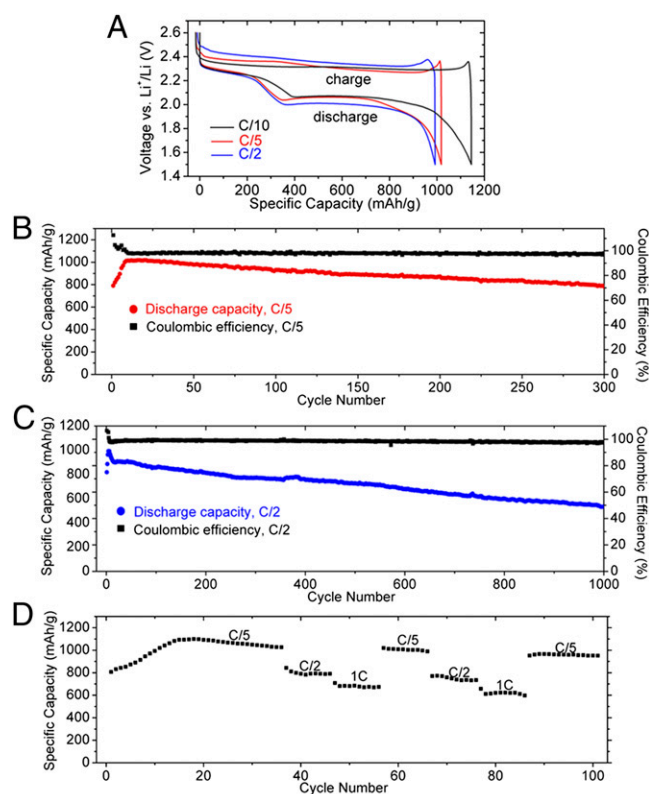


**Fig. 3.** Electrochemical characteristics of the PVP-encapsulated hollow S nanospheres. (A) Typical discharge–charge voltage profiles of the cell made from PVP-encapsulated hollow S nanosphere cathode at different current rates (C/10, C/5 and C/2, 1C = 1,673 mA/g) in the potential range of 2.6–1.5 V at room temperature. (B) Cycling performances and coulombic efficiency of the cell at a current rate of C/5 for 300 cycles. (C) Cycling performance and coulombic efficiency of the cell at a current rate of C/2 for 1,000 cycles. (D) Rate capability of the cell discharged at various current rates.

discharge capacity reached their highest, 1,018 mAh/g. A capacity of 931 mAh/g was retained after 100 cycles of charge/discharge, showing impressive capacity retention of 91.5% (of its highest discharge capacity of 1,018 mAh/g). A reversible capacity of around 790 mAh/g was still retained after 300 cycles, corresponding to a capacity retention of 77.6% of its highest capacity (a decay of only 7.8% per 100 cycles). The average coulombic efficiency of the cell at C/5 for 300 cycles is 98.08% (Fig. 3*B*).

When discharged/charged at C/2 rate (Fig. 3*C*), the cell also exhibits excellent cycling stability. After reaching its highest capacity of 990 mAh/g at the fourth cycle, the discharge capacity stabilized at 905 mAh/g after 10 more cycles. A discharge capacity of about 857 and 773 mAh/g can be obtained after 100 and 300 cycles, corresponding to capacity retention of 86.6% and 78.1% of its highest capacity, respectively. After 500 and 1,000 cycles, the cell delivered a reversible discharge capacity of 727 and 535 mAh/g, respectively, corresponding to capacity retention of 73.4% and 54.0% (of its highest capacity of 990 mAh/g). The capacity decay was as low as 0.046% per cycle. The cell also maintained a high coulombic efficiency even after 1,000 cycles (Fig. 3*C*), and the average over 1,000 cycles is about 98.5%.

The excellent cycling performance of the PVP-encapsulated hollow S nanospheres was reproducible over many coin cells. Another example of the electrochemical performance of the hollow S nanospheres electrode is demonstrated in Fig. 3*D*. The cell reached its highest capacity of 1,099 mAh/g after 18 cycles at C/5, and showed a stable reversible capacity of 1,026 mAh/g after 36 cycles. Further cycling at different rates (C/2 and 1C, each for

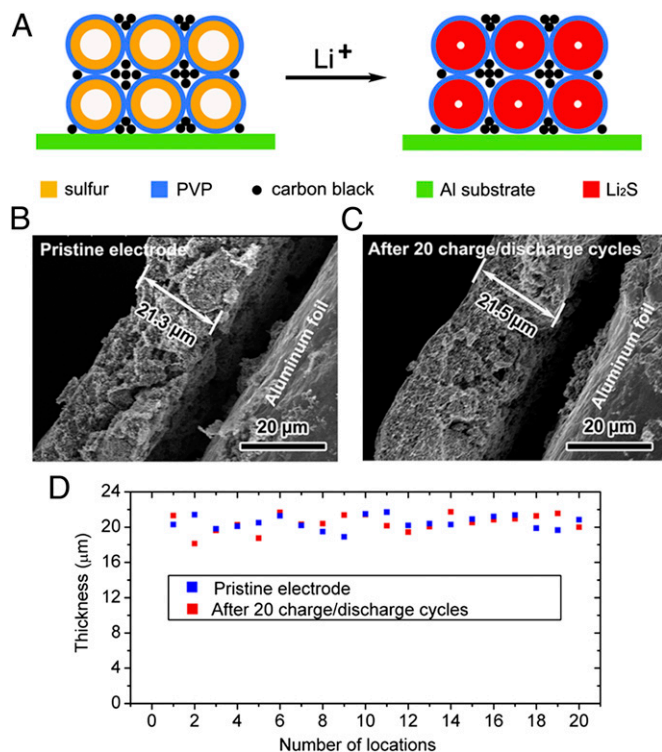


**Fig. 4.** Electrode thickness evaluation of the PVP-encapsulated hollow S nanosphere cathode. (A) Schematic illustrating that the electrode thickness would not change owing to the inward expansion of each of the hollow S nanospheres upon lithiation. (B and C) Typical SEM images of the cross-sections of hollow S nanosphere cathode, showing the thickness of (B) the pristine electrode and (C) the electrode after 20 charge/discharge cycles [at fully discharged (lithiated) state]. (D) A comparison of the thickness of 20 different locations for the cross-sections of the pristine electrode and the electrode after 20 charge/discharge cycles.

10 cycles) showed a reversible capacity of 800 mAh/g at C/2 and 674 mAh/g at 1C (a typical discharge/charge curve at 1C is shown in Fig. S6). When the cell was discharged at C/5 again, a reversible capacity of 989 mAh/g can be obtained after 10 more cycles, suggesting the high stability of the electrode. Even after another round of cycling at various current rates, a reversible capacity of about 953 mAh/g can still be retained at C/5 after 100 cycles, indicating superior capacity reversibility and good rate performance.

We further measured the S content dissolved in the electrolyte at the end of the 1st, 10th (after the activation process), and 500th cycle (at fully discharged state) at a current rate of C/5, which could provide the information about the degree of polysulfide dissolution. In a typical experiment, the coin cells were disassembled in argon-filled glove box, and then the components of the cells (cathode, anode, and separator) were washed with 1,3-dioxolane. This polysulfide-containing solution was oxidized with concentrated nitric acid and then diluted with deionized water for analysis of S content using inductively coupled plasma optical emission spectrometry (ICP-OES). For comparison, coin cells made from bare S particles were also disassembled and subjected to the same treatment. ICP analysis showed a loss of 81% of the total S mass into the electrolyte for bare S particles after the first discharge (the cycling performance of the cell made from hollow S nanospheres without PVP coating was shown in Fig. S7). In contrast, for the electrodes made from PVP-encapsulated hollow S nanospheres, only 16%, 19%, and 28% of the total S mass was found to be dissolved in the electrolyte after the 1st, 10th, and 500th cycle, respectively. This indicates effective

trapping of polysulfides by the PVP shells, although the perfect trapping still needs more work in the future.

The excellent electrochemical performance demonstrates that a design of monodisperse polymer-encapsulated hollow S nanoparticles combined with appropriate electrolyte additive can effectively address multiple materials issues. For battery materials with large volume change, the associated volume change propagating to the macroscopic scale of the whole electrode is a challenge. We can overcome this macroscopic expansion problem via the PVP-encapsulated hollow S nanospheres because the volume expansion is mitigated locally at each particle toward inside hollow space. Fig. 4A presents a schematic illustrating such a concept that the electrode thickness would not change. Fig. 4B and C show typical SEM images of the cross-sections of the cathode before and after 20 charge/discharge cycles [at C/5 rate, fully discharged (lithiated) state]. Fig. 4D shows the electrode thickness of 20 different locations for the cross-sections of the pristine electrode and the electrode after cycling, showing no signs of volume expansion at the whole electrode level. The result is very significant because it enables the simple design of the full battery.

Owing to the high monodispersity of the S nanospheres, further surface modifications on these particles become much easier than on microsized, irregularly shaped commercial S particles. Our previous study showed that mesoporous carbon/S composites wrapped with conducting polymer exhibited improved S cathode performance (39). By simply modifying the nanosphere surface with a thin layer of conducting polymer, poly(3,4-ethylenedioxythiophene) (PEDOT), based on a well-developed polymerization process (40), the S cathode performance can be further improved, especially the rate capability. Typical TEM image of the PEDOT-coated S nanospheres (Fig. 5A) shows that the hollow characteristic of the S nanospheres was preserved after the PEDOT coating. Fig. 5B clearly reveals the thickness of the PEDOT shell ( $\sim 16$  nm) after dissolving S by toluene. As shown in Fig. 5C, the electrode made from the PEDOT-coated S nanoparticles exhibited dramatically improved rate capabilities compared with the PVP-coated ones (Fig. 3D). This can be explained by the increase in reaction kinetics between lithium and S in the presence of the conductive polymer compared with the nonconductive one. EIS measurements on the cell made from PEDOT-coated S nanoparticles showed

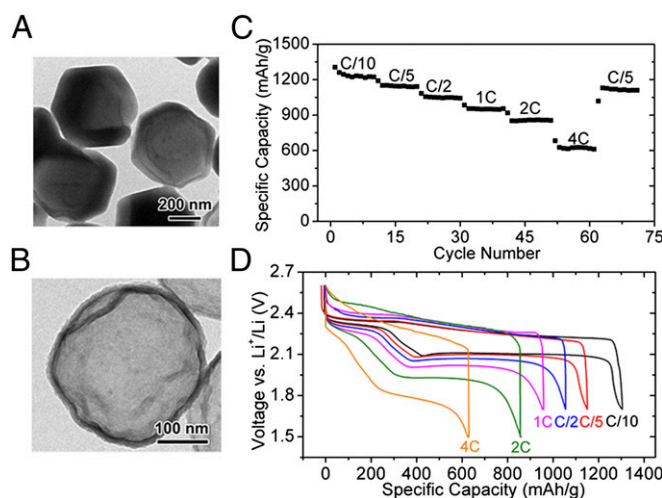


**Fig. 5.** TEM images and electrochemical characteristics of PEDOT-coated hollow S nanospheres. (A) TEM image of the PEDOT-coated hollow S nanospheres. (B) TEM image showing the PEDOT shell after dissolving S by toluene. (C) Rate capability of the PEDOT-coated S nanosphere cathode cycled at various current rates from C/10 to 4C. (D) Discharge-charge voltage profiles of PEDOT-coated S nanosphere cathode cycled at various current rates. Specific capacity values were calculated based on the mass of S.

## Materials and Methods

### Synthesis and Characterization of Polymer-Encapsulated Hollow S Nanospheres.

In a typical synthesis, 50 mL of 80 mM sodium thiosulfate ( $\text{Na}_2\text{S}_2\text{O}_3$ ; Aldrich) aqueous solution was mixed with 50 mL of 0.4 M PVP (molecular weight of  $\sim 55,000$ ; Aldrich; the concentration was calculated in terms of the repeating unit) at room temperature. Then, 0.4 mL of concentrated hydrochloric acid (HCl) was added to the  $\text{Na}_2\text{S}_2\text{O}_3$ /PVP solution under magnetic stirring. After

dramatically decreased charge transfer resistance during discharge compared with that made from the PVP encapsulated ones (Fig. S8). At C/10 rate, a reversible capacity of around 1,222 mAh/g is achieved after 10 cycles. Subsequent cycling at C/5, C/2, 1C, 2C, and 4C (each rate for 10 cycles) showed high reversible capacities of 1,140, 1,043, 947, 849, and 610 mAh/g, respectively. When the current was abruptly switched from 4C to C/5 again, a reversible capacity of 1,110 mAh/g can still be recovered, revealing the high stability of the electrode. Fig. 5D shows the voltage profiles of PEDOT-coated S nanospheres cycled at various current rates. The voltage hysteresis decreases compared with that of the PVP-coated particles (Fig. 3A).

In summary, we have successfully synthesized monodisperse, polymer-encapsulated hollow S nanospheres through a facile cost-effective, one-step, bottom-up synthesis method in aqueous solution at room temperature. We demonstrated that excellent S cathode performance can be achieved using these polymer-encapsulated hollow particles owing to their unique structural characteristics. As a highlight, we showed impressive cycling stability over 1,000 cycles with a capacity decay as low as  $\sim 0.46$  mAh/g per cycle. We believe that our simple, room temperature, scalable synthesis method and design of encapsulated hollow S nanospheres open up an exciting opportunity for next generation of low-cost and high-energy batteries.

## Materials and Methods

### Synthesis and Characterization of Polymer-Encapsulated Hollow S Nanospheres.

In a typical synthesis, 50 mL of 80 mM sodium thiosulfate ( $\text{Na}_2\text{S}_2\text{O}_3$ ; Aldrich) aqueous solution was mixed with 50 mL of 0.4 M PVP (molecular weight of  $\sim 55,000$ ; Aldrich; the concentration was calculated in terms of the repeating unit) at room temperature. Then, 0.4 mL of concentrated hydrochloric acid (HCl) was added to the  $\text{Na}_2\text{S}_2\text{O}_3$ /PVP solution under magnetic stirring. After

the reaction had proceeded at room temperature for 2 h, the solution was centrifuged at 7,000 rpm (Eppendorf, Rotor F-35-6-30) for 10 min to isolate the precipitate. In the washing process, the precipitate was washed with 0.8 M PVP aqueous solution once and centrifuged at 6,000 rpm (Eppendorf, Rotor F-35-6-30) for 15 min. The PEDOT modification on the S nanosphere surface was based on a previously described polymerization process (40). The as-prepared PVP-coated S nanospheres were dispersed in 100 mL of water, to which 110  $\mu\text{L}$  of EDOT monomer, 0.1 g of camphorsulfonic acid and 0.6 g of  $(\text{NH}_4)_2\text{S}_2\text{O}_8$  oxidant was added. The mixture solution was stirred at room temperature overnight and then centrifuged at 6,000 rpm (Eppendorf, Rotor F-35-6-30) for 10 min to isolate the precipitate. SEM images were taken using FEI XL30 Sirion SEM operated at an accelerating voltage of 5 kV. TEM imaging was performed on a FEI Tecnai G2 F20 X-TWIN TEM operated at 200 kV. ICP-OES was performed using a Thermo Scientific ICAP 6300 Duo View Spectrometer.

**Electrochemical Measurements.** The polymer-encapsulated hollow S nanosphere powder (dried overnight) was mixed with Super-P carbon black and polyvinylidene fluoride binder, with mass ratio of 70:20:10, in *N*-methyl-2-pyrrolidone solvent to produce electrode slurry. The slurry was coated onto an aluminum foil current collector using doctor blade and then dried in vacuum oven at 40  $^\circ\text{C}$  for 3 h to form the working electrode. The typical mass loading of active S was  $\sim 1$  mg/cm $^2$ . The 2032-type coin cells (MTI Corporation) were fabricated using the working electrode and Li metal foil as the counter electrode. The electrolyte was 1.0 M lithium bis(trifluoromethanesulfonyl) imide (LiTFSI) and 0.1 M  $\text{LiNO}_3$  in 1,3-dioxolane and 1,2-dimethoxyethane (volume ratio, 1:1). The coin cells were assembled inside an Ar-filled glove box. Galvanostatic measurements were made using MTI battery analyzers. The electrochemical impedance spectroscopy analysis was performed on a VMP3 potentiostat (Bio-logic) with amplitude of 10 mV in the frequency range of 200 kHz to 100 mHz.

**ACKNOWLEDGMENTS.** Y.C. acknowledges the support from the Department of Energy, Office of Basic Energy Sciences, Division of Materials Sciences and Engineering, under Contract DE-AC02-76SF00515, through the LDRD project of the SLAC National Accelerator Laboratory.

- Armand M, Tarascon JM (2008) Building better batteries. *Nature* 451(7179):652–657.
- Dunn B, Kamath H, Tarascon JM (2011) Electrical energy storage for the grid: A battery of choices. *Science* 334(6058):928–935.
- Whittingham MS (2004) Lithium batteries and cathode materials. *Chem Rev* 104(10):4271–4301.
- Goodenough JB, Kim Y (2010) Challenges for rechargeable Li batteries. *Chem Mater* 22(3):587–603.
- Chan CK, et al. (2008) High-performance lithium battery anodes using silicon nanowires. *Nat Nanotechnol* 3(1):31–35.
- Park MH, et al. (2009) Silicon nanotube battery anodes. *Nano Lett* 9(11):3844–3847.
- Magasinski A, et al. (2010) High-performance lithium-ion anodes using a hierarchical bottom-up approach. *Nat Mater* 9(4):353–358.
- Wu H, et al. (2012) Stable cycling of double-walled silicon nanotube battery anodes through solid-electrolyte interphase control. *Nat Nanotechnol* 7(5):310–315.
- Liu N, et al. (2012) A yolk-shell design for stabilized and scalable li-ion battery alloy anodes. *Nano Lett* 12(6):3315–3321.
- Li X, et al. (2012) Hollow core-shell structured porous Si-C nanocomposites for Li-ion battery anodes. *J Mater Chem* 22:11014–11017.
- Bruce PG, Freunberger SA, Hardwick LJ, Tarascon JM (2012) Li-O $_2$  and Li-S batteries with high energy storage. *Nat Mater* 11(1):19–29.
- Yang Y, et al. (2010) New nanostructured Li $_2$ S/silicon rechargeable battery with high specific energy. *Nano Lett* 10(4):1486–1491.
- Mikhaylik YV, Akridge JR (2004) Polysulfide shuttle study in the Li/S battery system. *J Electrochem Soc* 151:A1969–A1976.
- Ji XL, Nazar LF (2010) Li-S batteries: Advances in sulfur electrode. *J Mater Chem* 20:9821–9826.
- Barchasz C, Lepretre JC, Alloin F, Patoux S (2012) New insights into the limiting parameters of the Li/S rechargeable cell. *J Power Sources* 199:322–330.
- Shim J, Striebel KA, Cairns EJ (2002) The lithium/sulfur rechargeable cell: Effects of electrode composition and solvent on cell performance. *J Electrochem Soc* 149:A1321–A1325.
- Ji X, Lee KT, Nazar LF (2009) A highly ordered nanostructured carbon-sulphur cathode for lithium-sulphur batteries. *Nat Mater* 8(6):500–506.
- Jayaprakash N, Shen J, Moganty SS, Corona A, Archer LA (2011) Porous hollow carbon-sulfur composites for high-power lithium-sulfur batteries. *Angew Chem Int Ed Engl* 50(26):5904–5908.
- Kim J, et al. (2013) An advanced lithium-sulfur battery. *Adv Funct Mater* 23(8):1076–1080.
- Zheng G, Yang Y, Cha JJ, Hong SS, Cui Y (2011) Hollow carbon nanofiber-encapsulated sulfur cathodes for high specific capacity rechargeable lithium batteries. *Nano Lett* 11(10):4462–4467.
- Guo J, Xu Y, Wang C (2011) Sulfur-impregnated disordered carbon nanotubes cathode for lithium-sulfur batteries. *Nano Lett* 11(10):4288–4294.
- Ji L, et al. (2011) Porous carbon nano. ber-sulfur composite electrodes for lithium/sulfur cells. *Energy Environ Sci* 4:5053–5059.
- Elazari R, Salitra G, Garsuch A, Panchenko A, Aurbach D (2011) Sulfur-impregnated activated carbon fiber cloth as a binder-free cathode for rechargeable Li-S batteries. *Adv Mater* 23(47):5641–5644.
- Ji L, et al. (2011) Graphene oxide as a sulfur immobilizer in high performance lithium/sulfur cells. *J Am Chem Soc* 133(46):18522–18525.
- Wang H, et al. (2011) Graphene-wrapped sulfur particles as a rechargeable lithium-sulfur battery cathode material with high capacity and cycling stability. *Nano Lett* 11(7):2644–2647.
- Ji X, Evers S, Black R, Nazar LF (2011) Stabilizing lithium-sulphur cathodes using polysulphide reservoirs. *Nat Commun* 2:325.
- Evers S, Yim T, Nazar LF (2012) Understanding the nature of absorption/adsorption in nanoporous polysulfide sorbents for the Li-S battery. *J Phys Chem C* 116:19653–19658.
- Demir-Cakan R, et al. (2011) Cathode composites for Li-S batteries via the use of oxygenated porous architectures. *J Am Chem Soc* 133(40):16154–16160.
- Xiao L, et al. (2012) A soft approach to encapsulate sulfur: Polyaniline nanotubes for lithium-sulfur batteries with long cycle life. *Adv Mater* 24(9):1176–1181.
- Duong T (2003) *FreedomCAR Program R&D on Energy Storage Systems* (Department of Energy, Washington, DC). Available at [http://www1.eere.energy.gov/solar/pdfs/sda\\_03duong.pdf](http://www1.eere.energy.gov/solar/pdfs/sda_03duong.pdf). Accessed December 12, 2005.
- Elazari R, et al. (2010) Morphological and structural studies of composite sulfur electrodes upon cycling by HRTEM, AFM and Raman spectroscopy. *J Electrochem Soc* 157:A1131–A1138.
- Schuster J, et al. (2012) Spherical ordered mesoporous carbon nanoparticles with high porosity for lithium-sulfur batteries. *Angew Chem Int Ed Engl* 51(15):3591–3595.
- Seh ZW, et al. (2013) Sulphur-TiO $_2$  yolk-shell nanoarchitecture with internal void space for long-cycle lithium-sulphur batteries. *Nat Commun* 4:1331.
- Sun T, King HE (1996) Aggregation behavior in the semidilute poly(*N*-vinyl-2-pyrrolidone)/water system. *Macromolecules* 29:3175–3181.
- Qiu P, Mao C (2010) Biomimetic branched hollow fibers templated by self-assembled fibrous polyvinylpyrrolidone structures in aqueous solution. *ACS Nano* 4(3):1573–1579.
- Xia Y, Wei M, Lu Y (2009) One-step fabrication of conductive poly(3,4-ethylenedioxythiophene) hollow spheres in the presence of poly(vinylpyrrolidone). *Synth Met* 159:372–376.
- Aurbach D, et al. (2009) On the surface chemical aspects of very high energy density, rechargeable Li-sulfur batteries. *J Electrochem Soc* 156:A694–A702.
- Yuan L, Qiu X, Chen L, Zhu W (2009) New insight into the discharge process of sulfur cathode by electrochemical impedance spectroscopy. *J Power Sources* 189:127–132.
- Yang Y, et al. (2011) Improving the performance of lithium-sulfur batteries by conductive polymer coating. *ACS Nano* 5(11):9187–9193.
- Zhang X, MacDiarmid AG, Manohar SK (2005) Chemical synthesis of PEDOT nanofibers. *Chem Commun (Camb)* 42(42):5328–5330.